Evaluating the area and position accuracy of surface water paths obtained by flow direction algorithms

Zhenya Li[a,b], Tao Yang[a,*d], Chong-Yu Xu[c], Pengfei Shi[a,b], Bin Yong[a,b], Ching-sheng Huang[a], Chao Wang[e],

[a] *State Key Laboratory of Hydrology-Water Resources and Hydraulic Engineering, Center for Global Change and Water Cycle, Hohai University, Nanjing 210098, China;*

[b] *School of Earth Sciences and Engineering, Hohai University, Nanjing 210098, China;*

[c] *Department of Geosciences, University of Oslo, P.O. Box 1047 Blindern, 0316 Oslo, Norway*

[d] *National Cooperative Innovation Center for Water Safety & Hydro-Science, Hohai University, Nanjing 210098, China;*

[e] *Hydrology Program, Department of Earth and Environmental Science, New Mexico Institute of Mining and Technology, Socorro, NM 87801, USA*

Abstract: The surface water path (SWP) extracted from digital elevation model (DEM) by flow direction algorithms is widely employed to obtain a variety of topographic variables used in hydrological modeling. Accurate SWPs can facilitate understanding the underlying mechanisms of water movement on Earth's surface. However, the accuracy of extracted SWPs by different flow direction algorithms has not been systematically studied. In this work, two indicators are developed to measure the area and position errors of extracted SWPs relative to theoretical SWPs on four synthetic surfaces representing typical terrains of

[*]Corresponding author:

Dr. Tao Yang, Professor

State Key Laboratory of Hydrology-Water Resources and Hydraulic Engineering

Center for Global Change and Water Cycle

Hohai University, Nanjing 210098

The People's Republic of China

E-mail: tao.yang@hhu.edu.cn

natural watersheds. Based on the formulas of the synthetic surfaces, theoretical true SWP can be derived for any grid cell on the DEM discretized from the synthetic surfaces. Several widely used flow direction algorithms including three single flow direction (SFD) algorithms (i.e. D8, Rho8 and D8-LTD approaches) and three multiple flow direction (MFD) algorithms (i.e. FDFM, MFD-md and D∞ approaches) are implemented to extract SWPs. Results suggest that significant distinctions can be detected in SWPs extracted by different flow direction algorithms. The SWPs extracted by SFD algorithms are always one-dimensional non-dispersive lines because SFD algorithms allow only one flow direction at each grid cell. In contrast, the SWPs extracted by MFD algorithms show excessive artificial dispersion. The average area error of extracted SWPs ranges from 16.3% to 75.2% on different synthetic surfaces and the minimum is obtained by FDFM approach for all synthetic surfaces. The average position error falls in the range of 46.0% to 161.4%. The maximum is gained by D8 or FDFM approach, and the minimum by D8-LTD or D∞ approach. The cross compensation of SWP area induced by artificial dispersion leads to relatively high area accuracy but relatively low position accuracy of MFD algorithms. In addition, increasing DEM resolution without capturing more topographic variability can decrease the area and position accuracy due to error accumulation from more steps of flow direction calculation. Our findings provide a beneficial insight into applying SWP-derived topographic variables to hydrological modeling.

Keywords: Surface water path (SWP); flow direction algorithm; synthetic surfaces; artificial dispersion; area and position precision

1. Introduction

Topography is a dominant factor in determining the paths of surface water under the effect of gravity (Wolock and McCabe, 1995; Tarboton, 1997). The determined surface water paths (SWPs) have been widely employed to compute a variety of hydrological and geomorphological variables such as total dispersion area (TDA), topographic wetness index (TWI) and total contributing area (TCA) (Shin and Paik, 2017). These variables offer topographic information to a range of geological models including distributed hydrological models (Pourali et al., 2016; Yi et al., 2017; Wang et al., 2018), soil erosion models (Pradhan et al., 2017) and landscape evolution models (Paik, 2012). Thus, extracting SWPs based on topographic data has primary topographical and hydrological significance (Orlandini and Moretti, 2009).

Digital elevation model (DEM) is the numerical approximation of topographic elevation map (Meisels et al., 1995). The most common data structure for DEM is regular square grid (Costa-Cabral and Burges, 1994). In present, various flow direction algorithms have been created to extract SWP based on raster DEMs, such as the D8 approach (O'Callaghan and Mark, 1984), Rho8 approach (Depraetere, 1989) and D∞ approach (Tarboton, 1997). On raster DEM, any grid cell and its eight adjacent grid cells can form a 3×3 window as shown in Figure 1a. In each 3×3 window, a flow direction algorithm decides the flow direction of center grid cell and allocates the water from the center grid cell to the adjacent grid cells (Qin et al., 2007). The grid cell receiving water is called a "receiving grid cell". According to the number of receiving grid cells on a 3×3 window, flow direction algorithms can be classified into two types, namely single flow direction (SFD) and multiple flow direction (MFD) algorithms (Kok et al., 2018). An SFD algorithm allows only one receiving grid cell while an MFD algorithm allows multiple ones from each center grid cell (Qin et al., 2007).

The earliest and simplest SFD algorithm is the D8 approach (O'Callaghan and Mark, 1984). It treats the adjacent grid cell in the direction of the steepest slope as the receiving grid cell. Due to simplicity, D8 approach has been widely applied in terrain analysis (Carrara, 1988; Survila et al., 2016; Wilson et al, 2007). However, several drawbacks in D8 approach were discovered in case studies. Wolock and McCabe (1995) stated that flow direction obtained by D8 approach is diverted from its true path by a degree of -45 to 45.

Erskine et al (2006) found the occurrence of unrealistic parallel flow paths. To settle the above problems, great efforts have been made to modify D8 approach (e.g. Fairfield and Leymarie, 1991; Paik, 2008; Orlandini et al., 2003). Fairfield and Leymarie (1991) introduced a stochastic variable into D8 approach when calculating the slopes for diagonal gird cells. Paik (2003, 2008) tried to obtain more reasonable flow directions by maximizing the use of information stored in DEMs. Despite of these modifications, it is found that SFD algorithms cannot produce satisfactory results on dispersive terrains (Orlandini and Moretti, 2009). The reason is that water over a two-dimensional grid cell is treated as a zero-dimensional point source and is projected downslope by a one-dimensional line (Orlandini and Moretti, 2009; Shelef and Hilley, 2013).

Typical MFD algorithms include the FD8 approach (Freeman, 1991), D∞ approach and FD∞ approach (Seibert and McGlynn, 2007), etc. Many investigations demonstrated the superiority of MFD algorithms in generating more accurate topographic variables (Erskine et al., 2006; Zhou and Liu, 2002; Pilesjö and Hasan, 2014). Yet Costa-Cabral and Burges (1994) argued that the SWP extracted by an MFD algorithm is a discontinuous area comprising portions of different grid cells. Some works criticized that MFD algorithms often lead to excessive numerical dispersion (Tarbaton, 1997; Seibert and McGlynn, 2007). The dispersion is different from the physical dispersion inherent in transport processes and thus is called artificial dispersion. Orlandini et al. (2003, 2012) stressed that the artificial dispersion is not consistent with the morphological definition of the drainage area. Seibert and McGlynn (2007) deemed that the cross compensation of drainage area induced by artificial dispersion is the essential reason for highly precise topographic variables obtained by MFD algorithms.

As was discussed, both SFD and MFD algorithms have advantages and drawbacks. Many scholars have focused on finding a comparatively better approach for each specific case (Desmet and Govers, 1996; Huang and Lee, 2015; Rampi et al., 2014; Orlandini et al., 2012). Wolock and McCabe (1995) investigated the TWI distributions obtained by different flow direction algorithms. Erskine et al. (2006) compared several typical flow direction algorithms according to the patterns of TCA maps. Zhou and Liu (2002) quantified the errors of specific contributing area (SCA) obtained by flow direction algorithms on synthetic surfaces. It, however, can be noticed that errors in topographic variables are related not only to flow direction algorithms but also to other factors (Desmet and Govers, 1996; Marthews et al., 2015; Zhou et al., 2011). For example, SCA is associated with counter length and TWI is a function of SCA and terrain slope. It is, therefore, questionable to evaluate flow direction algorithms based on the precision of obtained topographic variables. In addition, most studies paid attention only to the value precision of obtained topographic variables (e.g. Zhou and Liu, 2002; Zhou et al., 2011; Yong et al., 2012). Seldom have evaluated the spatial position precision of these geographically meaningful variables.

Unlike other topographic variables obtained based on flow direction algorithms (i.e. SCA, TCA, TDA and TWI), SWP is a direct product of flow direction algorithm with no relation to other factors. Higher precision in the area of SWP ensures less errors in estimated topographic information such as SCA (Zhou and Liu, 2002; Qin et al., 2007), TWI (Sörensen et al., 2006), catchment area, pedologic variables (Florinsky et al., 2002), valley lines (Lindsay, 2003) and drainage networks (Turcotte et al., 2001). High precision in the spatial position of SWPs facilitates understanding the underlying mechanisms of transport processes associated with fluid motion on Earth's surface, e.g. routing process in hydrological cycle, nutrient and chemical transport, landslide and soil erosion (Costa-Cabral and Burges, 1994; Ren et al., 2018; Li et al., 2018; Wang et al., 2017; Shi et al., 2017; Yang et al., 2017). To the best of our knowledge, both the area and position precisions of extracted SWPs have not been studied systemically.

The purpose of this work is to develop a method for evaluating the SWPs extracted by flow direction algorithms. Raster DEMs discretized from synthetic surfaces are used to represent the typical local terrains of natural watersheds. Theoretical 'true' SWP is derived based on the formulas of synthetic surfaces and compared with the SWPs extracted by flow direction algorithms. Two indicators are created to measure the area and position errors of extracted SWPs compared to the theoretical SWPs. Numerical experiments are conducted on synthetic surfaces and natural terrains to evaluate the performances of extracted SWPs. The reasons for the advantages and drawbacks of typical flow direction algorithms are also discussed.

2. Methodology

2.1 Flow direction algorithms

Flow direction algorithms can be categorized into two classes according to the number of receiving grid cells they can generate for each grid cell, namely SFD and MFD algorithms (Yong et al., 2012). At each grid cell, the SFD algorithms generate one flow direction toward one downstream cell, while the MFD algorithms can generate multiple flow directions toward multiple downstream cells with different probabilities. Several representative SFD and MFD algorithms are described in this section.

2.1.1 Single flow direction (SFD) algorithms

The SFD algorithms evaluated in this work are D8, Rho8 and D8-LTD. In almost all SFD algorithms, a 3×3 window consisting of a center grid cell (cell 0) and its eight adjacent grid cells (cells 1 to 8) is used as the basic calculation unit (Figure 1a). Cells 2, 4, 6 and 8 are called cardinal grid cells of cell 0 and cells 1, 3, 4 and 7 are called diagonal grid cells.

In D8 approach, the slopes between the center and its adjacent grid cells are calculated by (O'Callaghan and Mark, 1984):

$$Slope = (z_0 - z_i)/L_i \qquad \mathrm{i} = 1, 2, \cdots, 8 \tag{1}$$

where z_i is the elevation of cell *i* and L_i is the projected horizontal distance from the center of cell 0 to the center of cell *i*. If the side length of each grid cell is L, L_i is equal to L for cardinal grid cells and $\sqrt{2}L$ for diagonal ones. Based on the D8 approach, Rho8 approach introduces a stochastic variable *rho* into equation (1) (Depraetere, 1989):

$$Slope = rho \cdot (z_0 - z_i)/L_i \qquad \mathrm{i} = 1, 2, \cdots, 8 \tag{2}$$

rho is 1 for cardinal grid cells and 1/(1-*r*) for diagonal grid cells where *r* is a random variable uniformly distributed between 0 and 1. In both D8 and Rho8 approaches, the gird cell in the steepest direction is identified as the receiving grid cell.

In D8-LTD approach, the 3×3 window in Figure 1a is divided into 8 planar triangular facets, as shown in Figure 1b (Orlandini et al., 2003). The elevations of the center, cardinal and diagonal gird cells in a triangular facet are denoted by e_0, e_1 and e_2, respectively. The gradient of the triangular facet can be represented by a vector (s_1, s_2) where s_1=(e_0- e_1)/L and s_2=(e_1- e_2)/L. The magnitude of the steepest slope is s=(s_1^2+ s_2^2)$^{0.5}$ and the flow direction expressed as the angle with the cardinal direction of the facet is r=arctan(s_2/s_1). The slope s and the flow direction r need to be modified as follows if r is not in the range between 0 and $\pi/4$. If r<0, set r equal to 0 and set s equal to s_1. If r >$\pi/4$, set r equal to $\pi/4$ and set s equal to s_2. (Tartoon, 1997). The facet with the steepest slope is chosen as the drainage facet, of which the cardinal and diagonal grid cells are selected as the two candidates of the receiving grid cell. D8-LTD approach uses ‘transversal deviation’ to select a receiving grid cell from the two candidates. As shown in Figure 1b, transversal deviation is defined as the least distance from the center of a candidate grid cell to the path along the flow direction originating from the center grid cell. The candidate with the least transversal deviation (LTD) is identified as the receiving grid cell. For details of the D8-LTD approach, please refer to Orlandini et al. (2003, 2009).

Given a starting grid cell, one can construct a 3×3 window centered at the starting grid cell. On the 3×3 window, a SFD algorithm can identify a receiving grid cell for the starting grid cell. The receiving grid cell is treated as the center grid cell of a new 3×3 window and the SFD algorithm is implemented continuously to find new receiving grid cells until the border of the study area or a sink (depression) is reached. Extracted SWP is a one-dimensional line sequentially connecting the starting gird cell and all receiving grid cells.

2.1.2 Multiple flow direction (MFD) algorithms

Three MFD algorithms including FDFM, MFD-md and D∞ approaches are discussed in this work. The 3×3 window in Figure 1a is still used as the basic calculation unit for the FDFM and MFD-md approaches. On a 3×3 window, all of the adjacent grid cells lower than the center grid cell are identified as receiving grid cells. The water in the center grid cell is distributed proportionally to the receiving grid cells according to the following equation (Quinn et al., 1991):

$$f_i = \max(0, {Slope_i}^p \cdot L_i) / \sum_{k=1}^{8} \max(0, {Slope_i}^p \cdot L_i) \quad (3)$$

where f_i is the proportion of water distributed from the center grid cell *0* to the adjacent grid cell i, $Slope_i$ is the slope from the center cell *0* to cell i, L_i is the effective counter length of cell i and p is an exponent. L_i is 0.5L for cardinal grid cells and 0.354L for diagonal grid cells. The exponent p in the FDFM approach is a fixed constant, e.g., 1.1 in Freeman (1991). p in the MFD-md approach is a variable adapting to local slope (Qin et al., 2007):

$$p = 8.9 \cdot \min(Slope_i, 1) + 1.1 \quad (4)$$

Similar to the D8-LTD approach, the triangular facet in Figure 1b is also used as the basic calculation unit for the D∞ approach. The slope and direction of each facet can be calculated in the same way as in the D8-LTD approach in section 2.1.1. In the D∞ approach, both the cardinal and diagonal grid cells of drainage facet (the facet with the steepest slope) is identified as receiving grid cells. The proportions of water distributed to the receiving grid cells are calculated based on the aspect of the drainage facet. For details of the D∞ approach, please refer to Tarboton (1997).

Given a starting grid cell, multiple receiving grid cells can be identified by MFD algorithms on the 3×3 window centered at the starting grid cell. Each receiving grid cell becomes the center of a new 3×3 window and the MFD algorithm is implemented parallelly on the newly-constructed 3×3 windows until the border of study area or a sink is reached. Clearly, the water in the starting grid cell may be dispersed to a large range of downslope area and the extracted SWP is a broad area instead of a one-dimensional line.

2.2 Theoretical 'true' surface water path on synthetic surfaces

Theoretically, the flow direction at any point is perpendicular to the elevation contour line. The theoretical true SWP for a given starting grid cell on a natural terrain and in coordinate system are shown in Figure 2. The enveloping flow lines of all the flow lines passing through the starting grid cell are marked as flow lines 1 and 2 in Figure 2. The area encircled by flow line 1, flow line 2, the starting grid cell and the borders of the study area is the theoretical true SWP.

Suppose a terrain surface with elevation $z=f(x, y)$. An elevation contour line can be expressed as $f(x,y)=c$, where c is the elevation of the contour line, x and y are the horizontal and vertical coordinates of a point on the contour line. The slope at a point is:

$$Slope = \sqrt{{f_x}^2 + {f_y}^2} \tag{5}$$

where f_x and f_y are the partial derivatives of the elevation with respect to x and y. The flow direction is:

$$Flow\ direction = \arctan(f_x/f_y) \tag{6}$$

The flow line passing through the point is denoted by $g(x, y)$ and satisfies:

$$f'(x,y) \cdot g'(x,y) = -1 \tag{7}$$

Solving the differential equation (7) obtains (Zhou and Liu 2002):

$$g(x,y) = \int -1/f'(x,y)dx = \int f_y/f_x\, dx \tag{8}$$

Given the vertex coordinates of a starting grid cell, the area of the theoretical 'true' SWP can be calculated by numerical integration.

A real-world DEM contains a variety of errors originating from DEM acquisition and production, data truncation and interpolation processes, and depression removing techniques (Grimaldi et al., 2005; Nardi et al. 2008). One type of manifestation of these errors are spurious sinks, depressions and pits in the DEM

(Grimaldi et al., 2004, 2007), which create discontinuities in the DEM-derived drainage patterns and can dramatically influence DEM-based simulations of drainage basin hydrological response. Zhou and Liu (2002) stated that the uncertainty in the real-world DEM itself often masks the inherent errors of flow direction algorithms. In addition, theoretical SWPs can hardly be extracted due to the complexity of real-world DEMs. All of the above discussions suggest that it is difficult to assess flow direction algorithms on a real-world DEM.

This work adopts synthetic surfaces instead of real-world DEMs to evaluate different flow direction algorithms. The reason is that the DEM created from a synthetic surface that has a definite mathematical function is error-free (Zhou and Liu, 2002) and that terrain attributes at any point of the synthetic surface can be solved analytically (Qin et al., 2013). In this work, dispersive, convergent, and plain terrains are represented by ellipsoid, inverse ellipsoid and inclined plane, respectively. In addition, saddle is employed to represent a combination of dispersive and convergent terrains. Table 1 shows the formulas of the synthetic surfaces as well as the general equations of flow lines.

2.3 Area and position error indicators for extracted SWP

In this paper, two metrics are proposed to measure the area and position errors of the extracted SWP as compared to the theoretical SWP. Figure 3 presents a sketch map of the theoretical and extracted SWPs on a 2×2 window. The theoretical SWP is the region encircled by the solid red lines and the extracted SWP is the region encircled by the solid black lines. It can be found that any grid cell on the 2×2 window can be divided into three areas of A_1, A_2 and A_3. A_1 is the area belonging to both the theoretical and extracted SWPs, A_2 is the area belonging to the theoretical SWP but not to the extracted SWP, and A_3 is the area belonging to the extracted SWP but not to the theoretical SWP. The magnitudes of A_1, A_2 and A_3 fall into the range of 0 to L^2.

For a grid cell, the areas of the theoretical and extracted SWPs equal to (A_1+A_2) and (A_1+A_3), respectively. The absolute area error of the extracted SWP inside the grid cell is $|(A_1+A_2)-(A_1+A_3)|=|A_2-A_3|$. On a synthetic surface consisting of N grid cells, the relative area error of the extracted SWP is obtained as:

$$E1 = \frac{\sum_{i=1}^{N}|A_2-A_3|}{\sum_{i=1}^{N}(A_1+A_2)} \quad (9)$$

where N is the total number of grid cells on the synthetic surface. The bias between the spatial positions of the theoretical and extracted SWPs inside a grid cell can be measured by A_2+A_3. Thus, the relative position error of the extracted SWP on a synthetic surface can be calculated by:

$$E2 = \frac{\sum_{i=1}^{N}(A_2+A_3)}{\sum_{i=1}^{N}(A_1+A_2)} \quad (10)$$

To the best of our knowledge, the area and position precisions of the SWPs extracted by flow direction algorithms have not be quantitatively evaluated on synthetic surfaces.

3. Results and discussions

3.1 Theoretical and extracted SWPs on synthetic surfaces

3.1.1 The features of the synthetic surfaces and the theoretical SWP area

The synthetic surfaces listed in Table 1 are all discretized into 30×30 DEM matrices. The 3-D graphics of the synthetic surfaces and the spatial patterns of the theoretical SWP area are shown in Figure 4. Square-rooted theoretical SWP area is used in Figures 4b, 4d and 4h for better presentation.

Ellipsoid is a dispersive surface and flow at any point on the surface is routed to the border of the ellipsoid along a flow line. In Figure 4b, square-rooted theoretical SWP area decreases from the ellipsoid center to the ellipsoid borders, with its isolines showing an uneven distribution of being dense inside and sparse outside. In addition, all of the isolines are concave in the cardinal directions of the ellipsoid center and convex in the diagonal directions. It indicates a larger spatial variation rate of the square-rooted theoretical SWP area along the cardinal directions than that along the diagonal directions. Inverse ellipsoid is convergent everywhere and flow at any point on the surface will converge to its center. The square-rooted theoretical SWP area increases from the ellipsoid center to the ellipsoid borders, with its isolines being a group of concentric rhombuses with uneven spatial distribution.

The direction of the steepest slope and the flow direction are identical at any point on an inclined plane (e.g. Figure 4e), leading to a series of parallel flow lines. In Figure 4f, the isolines of the theoretical SWP area are even-spaced broken lines with a deflection of 90 degree. The corners of the isolines are along a straight line, of which the slope is equal to that of the steepest slope of the inclined plane. On a saddle (Figure 4g), flow lines on the surface start from the borders at $x=\pm1500$ and end at the borders at $y=\pm1500$. In Figure 4h, the isolines of the square-rooted theoretical SWP area extend in the direction of *x* axis and concave toward saddle center in the direction of *y* axis. The degree of concavity is much more significant for the isolines near the saddle center than those near the saddle boundaries.

3.1.2 Spatial patterns of the theoretical and extracted SWPs

The SWPs of several selected starting grid cells on each of the synthetic surfaces are shown in Figure 5 to illustrate the spatial patterns of the theoretical and extracted SWPs. In each plot, red lines are the boundaries of the theoretical flow lines passing through a starting grid cell, as illustrated by the flow lines 1 and 2 in Figure 2. The area encircled by the red lines, the starting grid cell and the border of the theoretical terrain is the theoretical SWP. The assembly of grid cells in blue colors is the SWP extracted by a flow direction algorithm. For each grid cell in the extracted SWP of a starting grid cell, the color depth reflects the proportion of the grid cell area that is assigned to the flow path of a water parcel from the starting grid cell. A darker color means higher proportion.

3.1.2.1 Spatial patterns of the SWP on an ellipsoid

Three grid cells are chosen on the ellipsoid as the starting grid cells of the theoretical and extracted SWPs (Figure 5a). The theoretical SWP is a fan-shaped area and its width is always larger than the size of one grid cell. However, the SWPs extracted by the SFD algorithms (i.e. D8, Rho8 and D8-LTD approaches) are always one-dimensional lines without dispersion. This is caused by the underlying hypothesis of allowing only one flow direction at each grid cell in the SFD algorithms. Grid cell 1 is located in the diagonal direction of the ellipsoid center and the average direction of its theoretical SWP is in the diagonal direction (i.e. 45 degree). Grid cell 3 is located in the cardinal direction of the ellipsoid center, of which the theoretical SWP is symmetrical about *y* axis (i.e. 90 degree). Figure 5a reveals that all SFD algorithms can accurately trace the average directions of the theoretical SWPs for grid cells 1 and 3.

As to grid cell 2, the average direction of the theoretical SWP has an angle less than 45 degree with the diagonal or cardinal directions of the ellipsoid center. Clear distinctions can be recognized among the SWPs extracted by different SFD algorithms for grid cell 2. D8 SWP is extended along the diagonal direction, most of which is out of the theoretical SWP. The cause is related to the data structure of raster DEM. For the center grid cell on a 3×3 window, only one out of its eight adjacent grid cells is identified by the D8 approach as the receiving grid cell. The flow direction is therefore the multiple of 45 degree, resulting in an error of 0 to 45 degree between the real and the D8 flow directions. Rho8 approach uses a stochastic variable to modify D8 flow directions. It can be seen from Figure 5a that the Rho8 SWP is partially covered by the theoretical SWP and has less position error (E2=90.4%) than the D8 SWP (E2=112.7%). A drawback of the Rho8 approach is the non-reproducibility due to the introduction of randomness. A Rho8 SWP obtained in another run is likely to follow a completely different path compared with the Rho8 SWP shown in Figure 5a. The non-reproducibility severely limits the use of Rho8 approach in practical cases. In addition, the errors of flow directions are continuously accumulated in D8 and Rho8 approaches when the SWP goes downslope. To relieve this problem, D8-LTD approach adjusts flow direction by considering the upstream cumulative error in flow direction. The grid cell creating the least cumulative error is identified as the receiving grid cell. In Figure 5a, D8-LTD SWP can perfectly trace the average direction of the theoretical SWP for grid cell 2, thus achieves the least E1 (69.6%) and E2 (69.8%) compared with other SFD algorithms.

Different to SFD algorithms, MFD algorithms (i.e. FDFM, MFD-md and D∞ approaches) yield much more dispersive SWPs by allowing multiple flow directions at one grid cell. Most SWPs extracted by MFD algorithms are fan-shaped and can cover the theoretical SWPs. In FDFM SWPs, no large differences can be observed in the color depth of different grid cells with the same distance to the starting grid cell, meaning that these grid cells receive almost the same proportion of water from the starting grid cell. In contrast, there are main flow paths in MFD-md and D∞ SWPs, the color depth of which is obviously darker than that of the neighboring grid cells.

Besides, a large number of grid cells in the SWP extracted by the MFD algorithms do not belong to the theoretical SWP, indicating an overestimation of extracted SWP. The excessive dispersion is clearly different from the physical dispersion inherent in natural transport processes and thus is criticized as artificial dispersion. An essential reason for the occurrence of artificial dispersion is the defect of water allocation strategy in MFD algorithms. In FDFM and MFD-md approaches, the adjacent grid cells lower than the center grid cell are all treated as receiving grid cells on a 3×3 window. D∞ approach searches for the facet with the steepest slope, both the diagonal and the cardinal grid cells of which are identified as the receiving grid cells. Obviously, the above strategies are designed empirically without sufficient scientific evidences. The difference between man-made rules in MFD algorithms and natural rules in transport process leads to artificial dispersion. To minimize artificial dispersion, MFD-md approach adjusts the flow-partition exponent p in equation (3) and D∞ approach allows a maximum of two receiving grid cells. It can be observed in Figure 5a that artificial dispersion is effectively limited in the MFD-md and D∞ SWPs.

Most FDFM SWPs have the least area errors (i.e. least E1) compared to the SWPs extracted by other approaches. The position errors of FDFM SWPs are, however, always larger than those of MFD-md and D∞ SWPs. Particularly in the case of grid cell 2, the E2 of FDFM SWP (106.5%) is nearly twice as large as the E2s of MFD-md SWP (56.4%) and D∞ SWP (60.8%). The high area accuracy and low position accuracy of

FDFM SWPs can also be explained by artificial dispersion. As was discussed, a fraction of extracted SWP is out of theoretical SWP due to artificial dispersion. The area of the extracted SWP outside the theoretical SWP can crossly compensate the area deficit of the extracted SWP inside the theoretical SWP, which is called cross compensation. A larger artificial dispersion triggers stronger cross compensation, leading to less differences between the areas of the theoretical and extracted SWPs (i.e. less E1). Conversely, the spatial positions of the extracted SWP inside and outside the theoretical SWP cannot be compensated crossly. Enhancing artificial dispersion will increase the position error of the extracted SWP (i.e. larger E2).

3.1.2.2 Overall spatial patterns of SWPs on the synthetic surfaces

Because of allowing only one flow direction at each grid cell, the SWPs extracted by SFD algorithms are non-dispersive one-dimensional lines on all synthetic surfaces in Figure 5. It suggests to some extent that SFD algorithms may not be appropriate for dispersive terrains. It can be clearly found that D8 SWPs have a tendency to go straight along diagonal or cardinal directions for lack of a change to flow direction. Compared with D8 approach, Rho8 approach can generate SWPs closer to the theoretical SWPs for some grid cells (e.g. grid cell 2 on ellipsoid, grid cell 1 on inclined plane and grid cell 1 on saddle) than for the others (e.g. grid cell 1 on inverse ellipsoid and grid cell 3 on inclined plane). The instability in performance is caused by the introduction of randomness and restricts the further application of Rho8 approach in practical cases. D8-LTD SWPs can perfectly follow the average direction of theoretical SWPs on all synthetic surfaces, particularly inverse ellipsoid and inclined plane. Accordingly, D8-LTD SWPs show less position errors than the SWPs extracted by other approaches. The significant improvement in the position accuracy of D8-LTD SWPs benefits from the consideration of upstream accumulated deviations.

The underlying hypothesis of multiple flow directions in MFD algorithms creates dispersive SWPs in Figure 5. Particularly, the extracted SWPs are dispersed to a wide range of downslope area on convergent terrain (inverse ellipsoid in Figure 5b) and plane terrain (inclined plane in Figure 5c). Due to cross compensation induced by artificial dispersion, FDFM approach yields the least E1 and largest E2 on all synthetic surfaces except inverse ellipsoid. MFD-md and D∞ SWPs have nearly the same E1s and E2s for all starting grid cells, but D∞ SWPs present some distinctive features compared with MFD-md SWPs. In the case of grid cell 3 on ellipsoid, D∞ SWP is clustered in the right side of *y* axis while FDFM and MFD-md SWPs are symmetrical about *y* axis. As to grid cell 2 on saddle, D∞ SWP stays in the fourth quadrant while a fraction of FDFM and MFD-md SWPs spread to the second quadrant. The above differences can be partly explained by the way of identifying receiving grid cells in D∞ approach. The number of receiving grid cells is at most two in D∞ approach. As belong to the same triangular facet, the two receiving grid cells are adjacent to each other with an angle of 45 degree. In other words, the water of the center grid cell cannot be allocated to two grid cells with an angle larger than 45 degree. The spatial patterns of D∞ SWPs are, therefore, more centralized and asymmetric than those of FDFM and MFD-md SWPs.

3.1.3 Area and position accuracy of extracted SWPs on synthetic surfaces

Each gird cell in a DEM matrix can be regarded as a starting grid cell of SWP. Figures 6 to 9 show the spatial patterns of extracted SWP areas, area errors E1 and position errors E2 on different synthetic surfaces, respectively. The average E1 and E2 for all grid cells on synthetic surfaces are listed in Table 2.

On ellipsoid (i.e. in Figure 6), the isolines of extracted SWP area are convex in cardinal directions and concave in diagonal directions for almost all flow direction algorithms. The patterns are completely opposite to the patterns of theoretical isolines in Figure 4. The only exception is the FDFM approach, the isolines of which show more agreement with theoretical isolines. More blue grid cells and less red grid cells can be seen in the E1 distribution of FDFM approach, indicating an overall decrease in the area errors of extracted SWPs. Moreover, Table 2 reveals that the average E1 of FDFM approach (31.9%) is approximately 10% less than the average E1 of other approaches on ellipsoid. All the above findings prove that the areas of FDFM SWPs have the highest accuracy compared with the SWPs extracted by other approaches.

Large distinctions can be observed among the spatial distribution of E2 error for different flow direction algorithms. In the E2 distribution of D8 approach, there are eight feather-shaped dark red areas between neighboring cardinal and diagonal directions. The grid cell in dark red color generally has a position error of >120%. A number of dark red gird cells are turned into green or blue colors in the E2 distribution of Rho8 approach and nearly no dark red grid cells can be detected in the E2 distribution of D8-LTD approach. Table 2 reveals that the average position accuracy of Rho8 and D8-LTD approaches measured by E2 have an improvement of 10.6% and 32.5% over that of D8 approach. It suggests that the modifications to flow direction can effectively improve the position accuracy of extracted SWPs in Rho8 and D8-LTD approaches. The E2 distribution of FDFM approach has the largest red area with an average E2 (76.0%) second only to that of D8 approach (80.1%). The E2 distributions of MFD-md and D∞ approaches exhibit high similarities with that of D8 approach, but have less red area and lighter color.

Some of above findings are also true for other synthetic surfaces. In Figures 7 to 9, FDFM approach yields the least average E1 on all synthetic surfaces except inverse ellipsoid. This is the reason why FDFM approach is widely used to generate TWI maps in TOPMPDEL (Qiunn et al., 1991). High similarities in the E1 distributions and average E1s can be detected for other flow direction algorithms. On the other hand, the E2 distributions and average E2s of different approaches are obviously distinctive. The largest average E2 is obtained by D8 or FDFM approach whereas the least by D8-LTD or D∞ approach. It can be found in Table 2 that FDFM approach obtains the least average E1 and (secondary) largest average E2 on almost all synthetic surfaces. The reason is the cross compensation of area induced by artificial dispersion.

The average E1 ranges from 16.3% to 75.2% and the averaged E2 ranges from 46.0% to 161.4% on different synthetic surfaces. Most average E1s and E2s are larger than 20%, which may be not satisfactory in practice. It is therefore questionable to apply the topographic information extracted by these flow direction algorithms for topographical simulation. There is an urgent need of proposing a flow direction algorithm that can extract topographic information more accurately.

3.1.4 Impacts of DEM resolution on the average E1 and E2

The variations of average E1 and E2 with DEM resolution on synthetic surfaces are shown in Figure 10. In each sub-figure, the value of the *x* axis denotes the number of grid cells in the row or column of the DEM matrix discretized from synthetic surface. An increase in the value of *x* axis implies an increase in the resolution of DEM.

Given a flow direction algorithm, it can be seen in Figure 10 that increasing DEM resolution can lead to an increasing average E1 on ellipsoid, inclined plane and saddle, but a decreasing average E1 on inverse ellipsoid. The average E2 exhibits a positive correlation with DEM resolution on all synthetic surfaces. As DEM resolution is increased, the variation amplitudes of both the average E1 and E2 are reduced rapidly. Given a DEM resolution, flow direction algorithms generate similar average E1s (except FDFM approach) but obviously different average E2s. FDFM approach obtains the least average E1 and (secondary) largest average E2 for all DEM resolutions and synthetic surfaces. The largest average E2 is obtained by D8 approach in most cases.

Despite the fact that a DEM of a higher resolution can provide a better approximation of real terrains, extracted SWPs show lower area and position accuracy. Moreover, increasing DEM resolution can increase the computational burden exponentially. For example, while using D8 approach, it takes about 1 minute to extract SWPs on a 30×30 DEM matrix but more than 5 minutes on a 60×60 DEM matrix. We recommend that there is no need to refine the DEM resolution when a real terrain has been split into a collection of terrain units with simple forms (i.e. plane, convergent or dispersive terrains).

3.2 Spatial patterns of extracted SWPs on a real terrain

This section makes a qualitative analysis of the extracted SWPs on real terrains. A 30×30 DEM matrix is chosen from the Louhe Basin (110°20’, 34°7’), China. The DEM is downloaded from the Geospatial Data Cloud (http://www.gscloud.cn/) with a horizontal resolution of 30 m and a vertical resolution of 1 m. ArcGIS software is used for data pre-processing to remove topographic depressions and flat areas on DEM matrix. 3-dimensional plot of DEM in Figure 11 reveals that hillsides and valleys are crossly distributed over the study area. The extracted SWPs for several starting grid cells are presented in Figure 11.

Valley is a typical convergent local terrain in nature. In Figure 11a, two starting grid cells on valley lines are used as the starting grid cells of SWPs. Both the SFD and MFD algorithms can trace valley lines successfully and there are few distinctions in the SWPs extracted by different approaches. Notwithstanding, slight artificial dispersion can be detected in FDFM and FMD-md SWPs. Flow is exchanged between valley and hillside grid cells in the red circles of Figure 11a, which is clearly contrary to the laws of nature.

One of the most typical dispersive local terrains in nature is hillside. One grid cell on hillslope and one grid cell at the peak of a hillside are chosen as examples in Figure 11b. It can be observed that the SWPs extracted by SFD algorithms are all highly similar one-dimensional non-dispersive lines. In contrast, significant dispersion occurs in the SWPs extracted by MFD algorithms. FDFM SWP presents the greatest dispersion, followed by MFD-md SWP, and then D∞ SWP. In particular, FDFM SWP covers the whole hillside in the case of grid cell 4. Obvious main paths can be observed in the SWPs extracted by MFD algorithms, the color depth of which is much darker than the neighboring grid cells. The main paths are highly consistent with the one-dimensional SWPs extracted by SFD algorithms. D∞ SWPs show some obvious distinctions compared with the SWPs extracted by other MFD algorithms. For grid cell 3, D∞ SWP is concentrated on the left side of a hillside, yet the aspect of the hillside is due south and the true SWP should be right-and-left symmetrical. As to grid cell 4, D∞ SWP goes downslope along a path on the right side of hillside while FDFM and MFD-md SWPs are split into two main drainage paths at the starting grid cell. The distinctions, as was discussed, can be attributed to the way of identifying receiving grid cells in D∞

approach. The approach cannot find out two drainage directions with an angle > 45 degree. Comparatively, MFD-md approach has the best performances on dispersive terrains, the SWP of which has multiple drainage directions with limited artificial dispersion.

4. Conclusion

This work studies the accuracy of SWPs extracted by several representative flow direction algorithms on synthetic surfaces. A method is developed to calculate the theoretical 'true' SWP based on the formulas of synthetic surfaces. Two indicators are created to measure the area and position errors of extracted SWPs relative to the theoretical SWPs. Major findings are summarized as follows:

(1) The SWPs extracted by SFD algorithms are always one-dimensional non-dispersive lines due to the underlying hypothesis of allowing only one flow direction at each grid cell. D8 SWPs have a tendency to go straight along diagonal or cardinal direction for lack of a modification to flow direction. The theoretical and the D8 flow directions always differ by an angle of 0 to 45 degree. Rho8 approach uses a stochastic term to modify the flow direction. The introduction of randomness leads to more accurate SWPs for some grid cells but less accurate SWPs for some others. The instability of the performance seriously limits the use of Rho8 approach in practice. D8-LTD approach can accurately trace the average direction of theoretical SWPs, leading to a much higher position accuracy than other approaches. This benefits from the consideration of upstream accumulated deviations in D8-LTD approach.

(2) MFD algorithms yield excessive dispersive SWPs because of allowing multiple flow directions at each grid cell. The dispersion differs from the physical dispersion inherent in natural transport processes, thus is called artificial dispersion. An essential reason for the artificial dispersion is the difference between man-made rules in MFD algorithms and natural rules in physical transport process. The most significant artificial dispersion is always produced by FDFM approach, followed by MFD-md approach and then D∞

approach. Due to the cross compensation of SWP area induced by artificial dispersion, FDFM SWPs exhibit the highest area accuracy and (secondary) lowest position accuracy compared with the SWPs extracted by other approaches. As to D∞ approach, the receiving grid cells on a 3×3 window is restricted to no more than two neighboring grid cells. Therefore, D∞ approach cannot find two drainage directions with an angle lager than 45 degree at each grid cell, resulting in much more centralized and asymmetric SWPs than the other approaches. Comparatively, MFD-md approach yields better SWPs characterized by multiple drainage directions and limited dispersion.

(3) There are high similarities in the E1 spatial distributions and average E1s of all flow direction algorithms except FDFM approach. The average E1 ranges from 16.3% to 75.2% on different synthetic surfaces and the minimum is obtained by FDFM approach for all synthetic surfaces. This is the reason why FDFM approach is widely used to obtain TWI map in TOPMPDEL. Obvious distinctions can be detected in the E2 spatial distributions and average E2s of different approaches. The average position error falls in the range of 46.0% to 161.4%. The maximum is gained by either D8 or FDFM approach, and the minimum by either D8-LTD or D∞ approach.

(4) On a synthetic surface, an increase in DEM resolution without capturing more topographic variability generally leads to a decrease in the area and position accuracy of extracted SWPs. We recommend that there is no need to increase DEM resolution when most basic terrain types (plane, convergent or dispersive terrains) in a real-world terrain have been clearly captured by the DEM .

In conclusion, this work provides a beneficial insight into evaluating the accuracy of extracted SWPs on synthetic surfaces. Results reveal that the average area and position errors of the extracted SWPs is larger than 20% and 45% in most cases, which is fairly unsatisfying in practice. There is an urgent need to propose a new flow direction algorithm that can extract topographic information more accurately.

Acknowledgments: The work was jointly supported by grants from the National Natural Science Foundation of China (51809072, 51879068), a grant from the Fundamental Research Funds for the Central Universities (2019B16914), a grant from Key R&D Program of Ningxia (20175046802), and a grant from National Key Research and Development Program (2018YFC0407900), and the Research Council of Norway (FRINATEK Project 274310).

References:

Carrara, A., 1988. Drainage and divide networks derived from high-fidelity digital terrain models. In Quantitative Analysis of Mineral and Energy Resources. (pp. 581-597). Springer, Dordrecht.

Costa−Cabral, M.C., Burges, S.J., 1994. Digital elevation model networks (DEMON): A model of flow over hillslopes for computation of contributing and dispersal areas. Water Resources Research. 30(6), 1681-1692. https://doi.org/10.1029/93WR03512

Depraetere, C., 1989. Etude g6omorphom6trique du bassin-versant de Booro-Borotou• parfir d'un modulen um6fiqued e terrain: Structure et fonctionnement hydrop6dologique d'un petit bassinversant de savane humide; Equipe HYPERBAV, Collection Etudes et Theses, journ•e hydrop•dologique, Inst. Fr. de Rech. Sci. pour le E•vel. en Cooperation, ORSTOM, Montpellier

Desmet, P.J.J., Govers, G.,1996. Comparison of routing algorithms for digital elevation models and their implications for predicting ephemeral gullies. International Journal of Geographical Information Systems. 10(3), 311-331. https://doi.org/10.1080/02693799608902081

Erskine, R.H., Green, T.R., Ramirez, J.A., MacDonald, L.H., 2006. Comparison of grid-based algorithms for computing upslope contributing area. Water Resources Research. 42(9). https://doi.org/10.1029/2005WR004648

Fairfield, J., Leymarie, P., 1991. Drainage networks from grid digital elevation models. Water Resources Research. 27(5), 709-717. https://doi.org/10.1029/90WR02658

Florinsky, I. V., Eilers, R. G., Manning, G. R., Fuller, L. G., 2002. Prediction of soil properties by digital terrain modelling.

Environmental Modelling & Software. 17(3), 295-311. https://doi.org/10.1016/S1364-8152(01)00067-6

Freeman, T.G., 1991. Calculating catchment area with divergent flow based on a regular grid. Computers & Geosciences. 17(3), 413-422. https://doi.org/10.1016/0098-3004(91)90048-I

Grimaldi, S., Teles, V., Bras, R. L., 2004. Sensitivity of a physically based method for terrain interpolation to initial conditions and its conditioning on stream location. Earth Surface Processes and Landforms: The Journal of the British Geomorphological Research Group, 29(5), 587-597. https://doi.org/10.1002/esp.1053

Grimaldi, S., Teles, V., Bras, R. L., 2005. Preserving first and second moments of the slope area relationship during the interpolation of digital elevation models. Advances in Water Resources, 28(6), 583-588. https://doi.org/10.1016/j.advwatres.2004.11.014

Grimaldi, S., Nardi, F., Di Benedetto, F., Istanbulluoglu, E., Bras, R. L., 2007. A physically-based method for removing pits in digital elevation models. Advances in Water Resources, 30(10), 2151-2158. https://doi.org/10.1016/j.advwatres.2006.11.016

Huang, P. C., Lee, K.T., 2015. Distinctions of geomorphological properties caused by different flow-direction predictions from digital elevation models. International Journal of Geographical Information Science. 30(2), 168-185. https://doi.org/10.1080/13658816.2015.1079913

Kok, K., Sidek, L.M., Jung, K., Kim, J., 2018. Analysis of runoff aggregation structures with different flow direction methods under the framework of power law distribution. Water Resources Management. 32(14), 4607-4623. https://doi.org/10.1080/13658816.2015.1079913

Li, Z., Yang, T., Huang, C. S., Xu, C. Y., Shao, Q., Shi, P., Wang, X.Y., Cui, T.,2018. An improved approach for water quality evaluation: TOPSIS-based informative weighting and ranking (TIWR) approach. Ecological Indicators. 89, 356-364. https://doi.org/10.1016/j.ecolind.2018.02.014

Lindsay, J. B., 2003. A physically based model for calculating contributing area on hillslopes and along valley bottoms. Water Resources Research. 39(12). https://doi.org/10.1029/2003WR002576

Marthews, T., Dadson, S., Lehner, B., Abele, S., Gedney, N., 2015. High-resolution global topographic index values for use in large-scale hydrological modelling. Hydrology and Earth System Sciences. 19(1), 91-104. https://doi.org/10.5194/hess-19-91-2015

Meisels, A., Raizman, S., Karnieli, A., 1995. Skeletonizing a DEM into a drainage network. Computers & Geosciences. 21(1), 187-196. https://doi.org/10.1016/0098-3004(94)00065-3

Nardi, F., Grimaldi, S., Santini, M., Petroselli, A., Ubertini, L., 2008. Hydrogeomorphic properties of simulated drainage patterns using digital elevation models: the flat area issue. Hydrological Sciences Journal, 53(6), 1176-1193. https://doi.org/10.1623/hysj.53.6.1176

O'Callaghan, J.F., Mark, D.M., 1984. The extraction of drainage networks from digital elevation data. Computer Vision, Graphics, and Image Processing. 28(3), 323-344. https://doi.org/10.1016/S0734-189X(84)80011-0

Orlandini, S., Moretti, G., Franchini, M., Aldighieri, B., Testa, B., 2003. Path-based methods for the determination of nondispersive drainage directions in grid-based digital elevation models. Water Resources Research. 39(6). https://doi.org/10.1029/2002WR001639

Orlandini, S., Moretti, G., 2009. Determination of surface flow paths from gridded elevation data. Water Resources Research. 45(3). https://doi.org/10.1029/2008WR007099

Orlandini, S., Moretti, G., Corticelli, M.A., Santangelo, P.E., Capra, A., Rivola, R., Albertson, J.D., 2012. Evaluation of flow direction methods against field observations of overland flow dispersion. Water Resources Research. 48(10). https://doi.org/10.1029/2012WR012067

Paik, K., 2008. Global search algorithm for nondispersive flow path extraction. Journal of Geophysical Research: Earth Surface, 113(F4). https://doi.org/10.1029/2007JF000964

Paik, K., 2012. Simulation of landscape evolution using a global flow path search method. Environmental Modelling & Software. 33, 35-47. https://doi.org/10.1016/j.envsoft.2012.01.005

Pilesjö, P., Hasan, A., 2014. A triangular form-based multiple flow algorithm to estimate overland flow distribution and accumulation on a digital elevation model. Transactions in GIS. 18(1), 108-124. https://doi.org/10.1111/tgis.12015

Pourali, S. H., Arrowsmith, C. Chrisman, N., Matkan, A. A., Mitchell, D., 2016. Topography wetness index application in flood-risk-based land use planning. Applied Spatial Analysis and Policy. 9(1), 39-54. https://doi.org/ 10.1007/s12061-014-9130-2

Pradhan, A.M.S., Kang, H.S., Lee, S., Kim, Y.T., 2017. Spatial model integration for shallow landslide susceptibility and its runout using a GIS-based approach in Yongin, Korea. Geocarto International. 32(4), 420-441. https://doi.org/10.1080/10106049.2016.1155658

Qin, C., Zhu, A.X., Pei, T., Li, B., Zhou, C., Yang, L., 2007. An adaptive approach to selecting a flow - partition exponent for a multiple−flow−direction algorithm. International Journal of Geographical Information Science. 21(4), 443-458. https://doi.org/10.1080/13658810601073240

Qin, C. Z., Bao, L. L., Zhu, A. X., Hu, X. M., Qin, B., 2013. Artificial surfaces simulating complex terrain types for evaluating grid-based flow direction algorithms. International Journal of Geographical Information Science, 27(6), 1055-1072. https://doi.org/10.1080/13658816.2012.737920

Quinn, P. F. B. J., Beven, K., Chevallier, P., Planchon, O., 1991. The prediction of hillslope flow paths for distributed hydrological modelling using digital terrain models. Hydrological Processes, 5(1), 59-79. https://doi.org/10.1002/hyp.3360050106

Quinn, P., Beven, K., Lamb, R., 1995. The in (a/tan/β) index: How to calculate it and how to use it within the topmodel framework. Hydrological Processes. 9(2), 161-182. https://doi.org/10.1002/hyp.3360090204

Rampi, L.P., Knight, J.F., Lenhart, C.F., 2014. Comparison of flow direction algorithms in the application of the CTI for mapping wetlands in Minnesota. Wetlands. 34(3), 513-525. https://doi.org/ 10.1007/s13157-014-0517-2

Ren, W., Yang, T., Shi, P., Xu, C. Y., Zhang, K., Zhou, X., Shao, Q.X., Ciais, P., 2018. A probabilistic method for streamflow projection and associated uncertainty analysis in a data sparse alpine region. Global and Planetary Change.165, 100-113. https://doi.org/10.1016/j.gloplacha.2018.03.011

Shelef, E., Hilley, G.E., 2013. Impact of flow routing on catchment area calculations, slope estimates, and numerical simulations of landscape development. Journal of Geophysical Research: Earth Surface. 118(4), 2105-2123. https://doi.org/10.1002/jgrf.20127

Seibert, J., McGlynn, B.L., 2007. A new triangular multiple flow direction algorithm for computing upslope areas from gridded digital elevation models. Water Resources Research. 43(4). https://doi.org/10.1029/2006WR005128

Shi, P., Yang, T., Xu, C. Y., Yong, B., Shao, Q., Li, Z., Wang, X.Y, Zhou, X.D., Li, S.,2017. How do the multiple large-scale climate oscillations trigger extreme precipitation?. Global and Planetary Change. 157, 48-58. https://doi.org/10.1016/j.gloplacha.2017.08.014

Shin, S., Paik, K., 2017. An improved method for single flow direction calculation in grid digital elevation models. Hydrological Processes. 31(8), 1650-1661. https://doi.org/10.1002/hyp.11135

Sörensen, R., Zinko, U., Seibert, J., 2006. On the calculation of the topographic wetness index: evaluation of different methods based on field observations. Hydrology and Earth System Sciences Discussions.10(1), 101-112. https://doi.org/ 10.5194/hess-10-101-2006

Survila, K., Yıldırım, A. A., Li, T., Liu, Y. Y., Tarboton, D. G., Wang, S., 2016. A scalable high-performance topographic flow direction algorithm for hydrological information analysis. In Proceedings of the XSEDE16 Conference on Diversity, Big Data, and Science at Scale (p. 11). ACM. https://doi.org/ 10.1145/2949550.2949571

Tarboton, D.G., 1997. A new method for the determination of flow directions and upslope areas in grid digital elevation models. Water Resources Research. 33(2), 309-319. https://doi.org/10.1029/96WR03137

Turcotte, R., Fortin, J. P., Rousseau, A. N., Massicotte, S., Villeneuve, J. P., 2001. Determination of the drainage structure of a watershed using a digital elevation model and a digital river and lake network. Journal of hydrology. 240(3-4), 225-242. https://doi.org/10.1016/S0022-1694(00)00342-5

Wang, C., Gomez-Velez, J. D., Wilson J. L., 2018. The Importance of Capturing Topographic Features for Modeling Groundwater Flow and Transport in Mountainous Watersheds. Water Resources Research. 54 (12), 10,313-10,338.

https://doi.org/10.1029/2018WR023863.

Wang, X., Yang, T., Wortmann, M., Shi, P., Hattermann, F., Lobanova, A., Aich, V., 2017. Analysis of multi-dimensional hydrological alterations under climate change for four major river basins in different climate zones. Climatic Change. 141(3), 483-498. https://doi.org/ 10.1007/s10584-016-1843-6

Wilson, J. P., Lam, C. S., Deng, Y., 2007. Comparison of the performance of flow−routing algorithms used in GIS‐based hydrologic analysis. Hydrological Processes. 21(8), 1026-1044. https://doi.org/10.1002/hyp.6277

Wolock, D.M., McCabe Jr, G.J, 1995. Comparison of single and multiple flow direction algorithms for computing topographic parameters in TOPMODEL. Water Resources Research. 31(5), 1315-1324. https://doi.org/10.1029/95WR00471

Yi, L., Zhang, W.C., Yan, C.A., 2017. A modified topographic index that incorporates the hydraulic and physical properties of soil. Hydrology Research. 48(2), 370-383. https://doi.org/10.2166/nh.2016.119

Yang, T., Cui, T., Xu, C. Y., Ciais, P., Shi, P., 2017. Development of a new IHA method for impact assessment of climate change on flow regime. Global and Planetary Change. 156, 68-79. https://doi.org/10.1016/j.gloplacha.2017.07.006

Yong, B., Ren, L.L., Hong, Y., Gourley, J.J., Chen, X., Zhang, Y.J., Yang, X.L., Zhang, Z.X., Wang, W.G., 2012. A novel multiple flow direction algorithm for computing the topographic wetness index. Hydrology Research. 43(1-2), 135-145. https://doi.org/10.2166/nh.2011.115

Zhou, Q., Liu, X., 2002. Error assessment of grid-based flow routing algorithms used in hydrological models. International Journal of Geographical Information Science. 16(8), 819-842. https://doi.org/10.1080/13658810210149425

Zhou, Q., Pilesjö, P., Chen, Y., 2011. Estimating surface flow paths on a digital elevation model using a triangular facet network. Water Resources Research. 47(7). https://doi.org/10.1029/2010WR009961

Table 1 Formulas of synthetic surfaces , general equations of flow lines and the constants in the formulas of the synthetic surfaces

	Formulas of synthetic surfaces	General equations of flow lines	Constants in the formulas of synthetic surfaces
Ellipsoid	$\frac{x^2}{a^2}+\frac{y^2}{b^2}+\frac{z^2}{c^2}=1(z>0)$	$y=cont\cdot x^{\frac{a^2}{b^2}}$	a=1600;b=1600;c=2000
Inverse Ellipsoid	$\frac{x^2}{a^2}+\frac{y^2}{b^2}+\frac{z^2}{c^2}=1(z<0)$	$y=cont\cdot x^{\frac{a^2}{b^2}}$	a=1600;b=1600;c=2000
Inclined Plane	$z=ax+by+c$	$y=\frac{b}{a}x+cont$	a=2;b=1.5;c=100
Saddle	$\frac{z^2}{c^2}=\frac{x^2}{a^2}-\frac{y^2}{b^2}$	$y=cont\cdot x^{\frac{a^2}{b^2}}$	a=1.5;b=1.0;c=0.1

Note: *cont* in the general equation of flow line is obtained by substituting point coordinates into the equation

Table 2 Average E1 and E2 obtained by SFD and MFD algorithms on different synthetic surfaces

	SFD algorithms			MFD algorithms		
	D8	Rho8	D8-LTD	FDFM	FMD-md	D∞
Average E1						
Ellipsoid	43.5%	41.7%	42.1%	31.9%	42.4%	43.1%
Inverse ellipsoid	46.2%	46.2%	47.6%	75.2%	47.3%	46.2%
Plane	47.4%	41.2%	41.0%	20.1%	43.6%	42.9%
Saddle	23.3%	23.4%	23.4%	16.3%	23.4%	23.5%
Average E2						
Ellipsoid	80.1%	69.5%	47.5%	76.0%	56.0%	55.9%
Inverse ellipsoid	161.4%	139.8%	100.7%	142.1%	96.1%	88.8%
Plane	115.4%	90.7%	48.6%	101.1%	84.4%	75.4%
Saddle	107.7%	90.8%	46.0%	97.5%	65.5%	61.0%

Figure captions

Figure 1 A 3×3 window in flow direction algorithm

Figure 2 Sketch map of theoretical SWP originating from a grid cell on a natural terrain and in coordinate system

Figure 3 Sketch map of the theoretical and estimated SWPs on 2×2 window

Figure 4 Spatial distributions of elevations and theoretical SWPs on theoretical terrains

Figure 5 Positions of theoretical and extracted SWPs on (a) ellipsoid, (b) inverse ellipsoid, (c) inclined plane and (d) saddle

Figure 6 Spatial distributions of extracted SWP area, E1 and E2 on ellipsoid

Figure 7 Spatial distributions of extracted SWP area, E1 and E2 on inverse ellipsoid

Figure 8 Spatial distributions of extracted SWP area, E1 and E2 on inclined plane

Figure 9 Spatial distributions of extracted SWP area, E1 and E2 on saddle

Figure 10 Variation of average E1 and E2 with the resolution of DEM matrices

Figure 11 SWPs extracted by SFD and MFD algorithms on (a) natural convergent terrains and (b) natural dispersive terrains

Figure 1

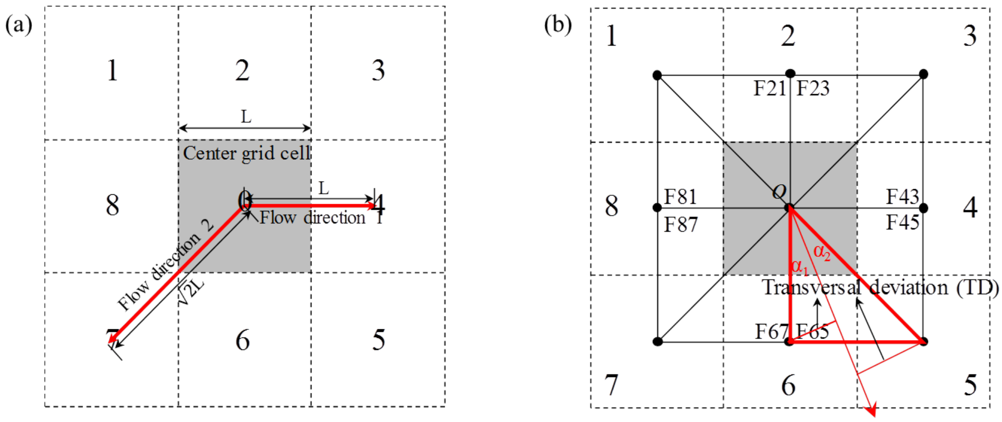

(a)
1
2
3
L
Center grid cell
8
0
L
4
Flow direction 1
Flow direction 2
√2L
7
6
5
(b)
1
2
3
F21
F23
8
F81
F87
O
F43
F45
4
α2
α1
Transversal deviation (TD)
F67
F65
7
6
5

Figure 2

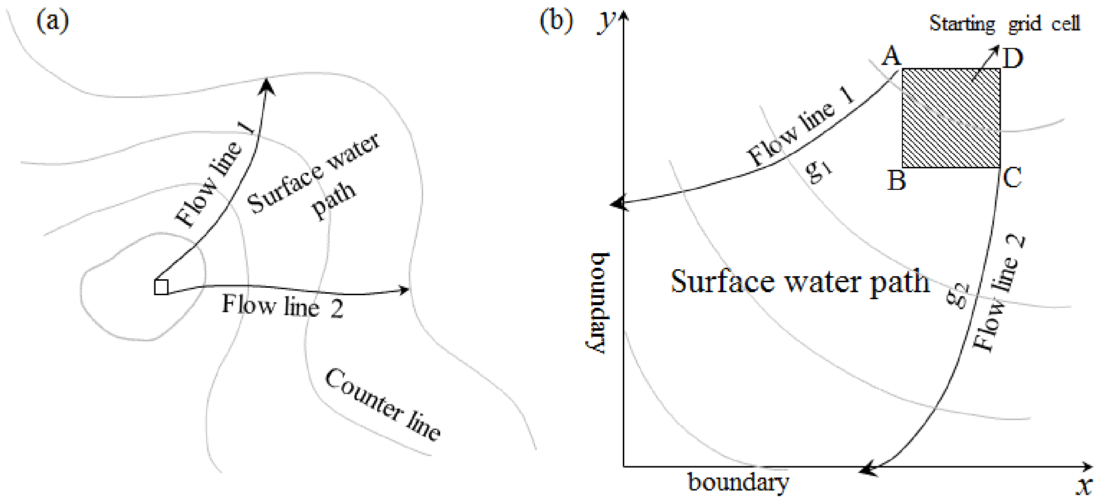

(a)
Flow line 1
Surface water path
Flow line 2
Counter line
(b)
y
Starting grid cell
A
D
B
C
Flow line 1
g_1
boundary
Surface water path
g_2
Flow line 2
boundary
x

Figure 3

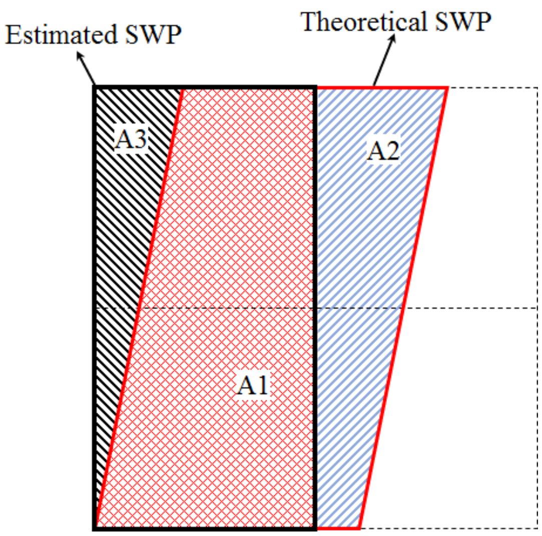

Figure 4

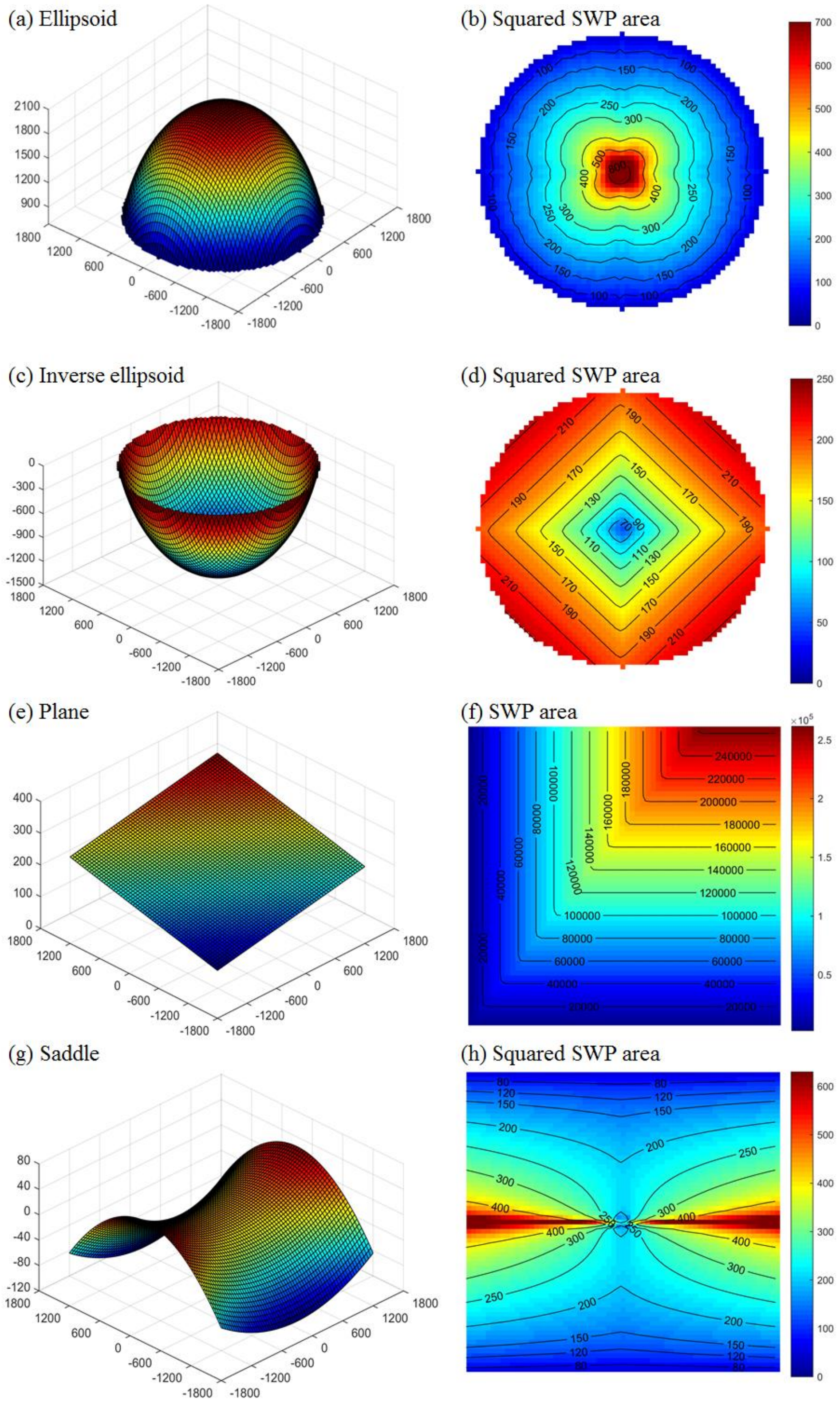
(a) Ellipsoid
(b) Squared SWP area
(c) Inverse ellipsoid
(d) Squared SWP area
(e) Plane
(f) SWP area
(g) Saddle
(h) Squared SWP area

Figure 5

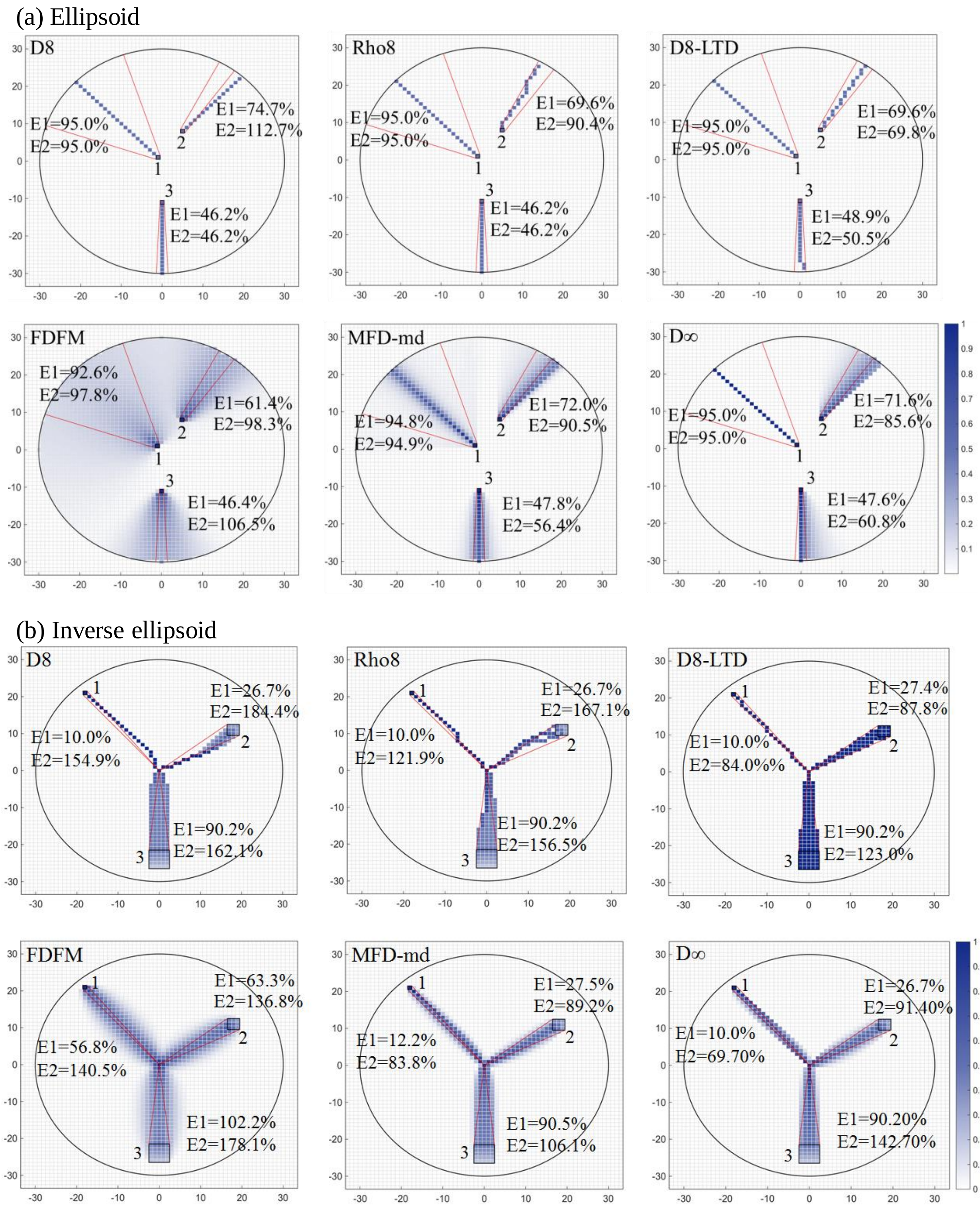

(a) Ellipsoid
D8
E1=95.0%
E2=95.0%
E1=74.7%
E2=112.7%
E1=46.2%
E2=46.2%
Rho8
E1=95.0%
E2=95.0%
E1=69.6%
E2=90.4%
E1=46.2%
E2=46.2%
D8-LTD
E1=95.0%
E2=95.0%
E1=69.6%
E2=69.8%
E1=48.9%
E2=50.5%
FDFM
E1=92.6%
E2=97.8%
E1=61.4%
E2=98.3%
E1=46.4%
E2=106.5%
MFD-md
E1=94.8%
E2=94.9%
E1=72.0%
E2=90.5%
E1=47.8%
E2=56.4%
D∞
E1=95.0%
E2=95.0%
E1=71.6%
E2=85.6%
E1=47.6%
E2=60.8%
(b) Inverse ellipsoid
D8
E1=10.0%
E2=154.9%
E1=26.7%
E2=184.4%
E1=90.2%
E2=162.1%
Rho8
E1=10.0%
E2=121.9%
E1=26.7%
E2=167.1%
E1=90.2%
E2=156.5%
D8-LTD
E1=10.0%
E2=84.0%%
E1=27.4%
E2=87.8%
E1=90.2%
E2=123.0%
FDFM
E1=56.8%
E2=140.5%
E1=63.3%
E2=136.8%
E1=102.2%
E2=178.1%
MFD-md
E1=12.2%
E2=83.8%
E1=27.5%
E2=89.2%
E1=90.5%
E2=106.1%
D∞
E1=10.0%
E2=69.70%
E1=26.7%
E2=91.40%
E1=90.20%
E2=142.70%

(c) Inclined plane

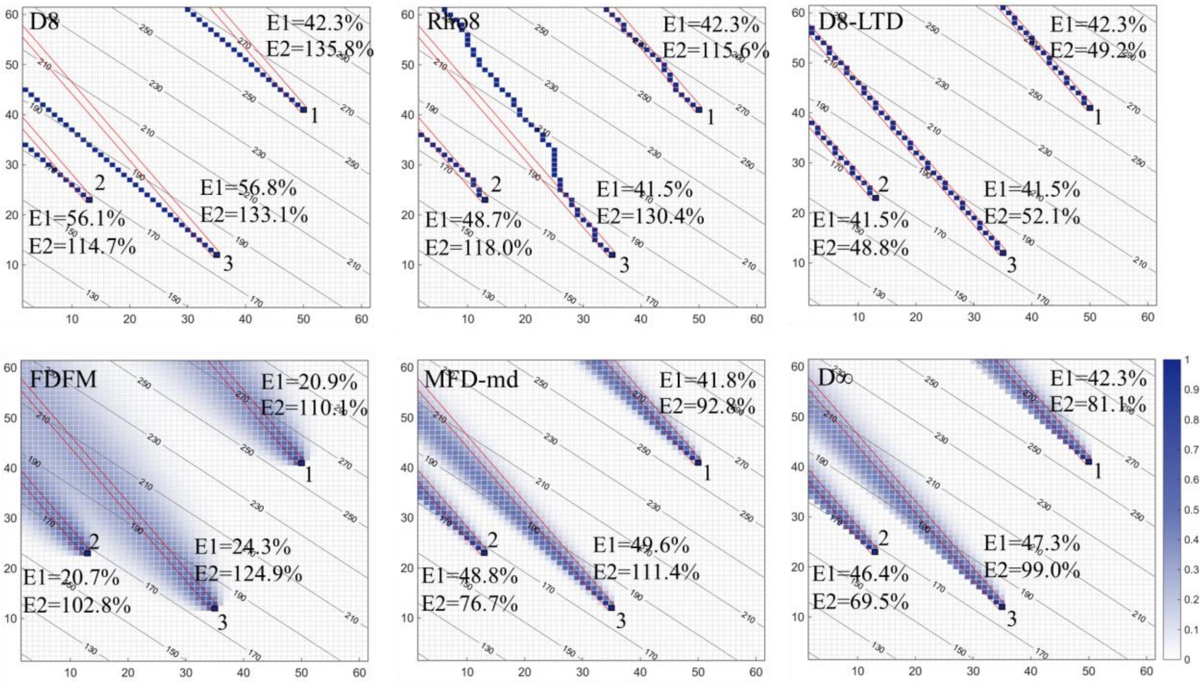

(d) Saddle

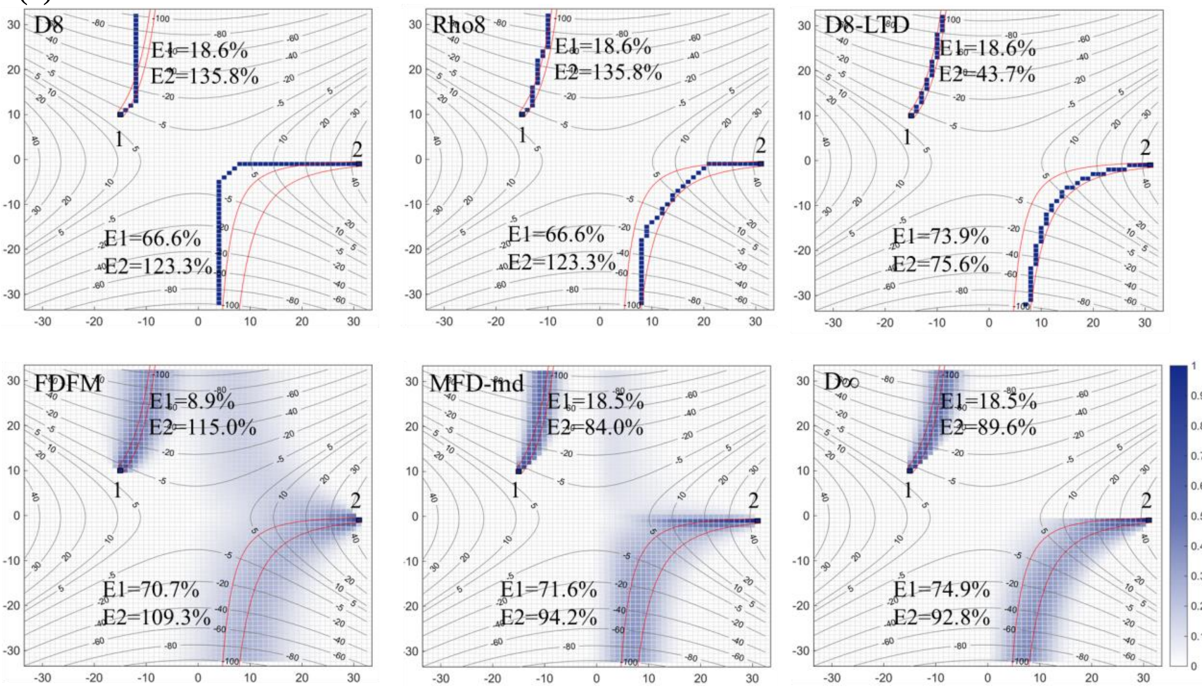

Figure 6

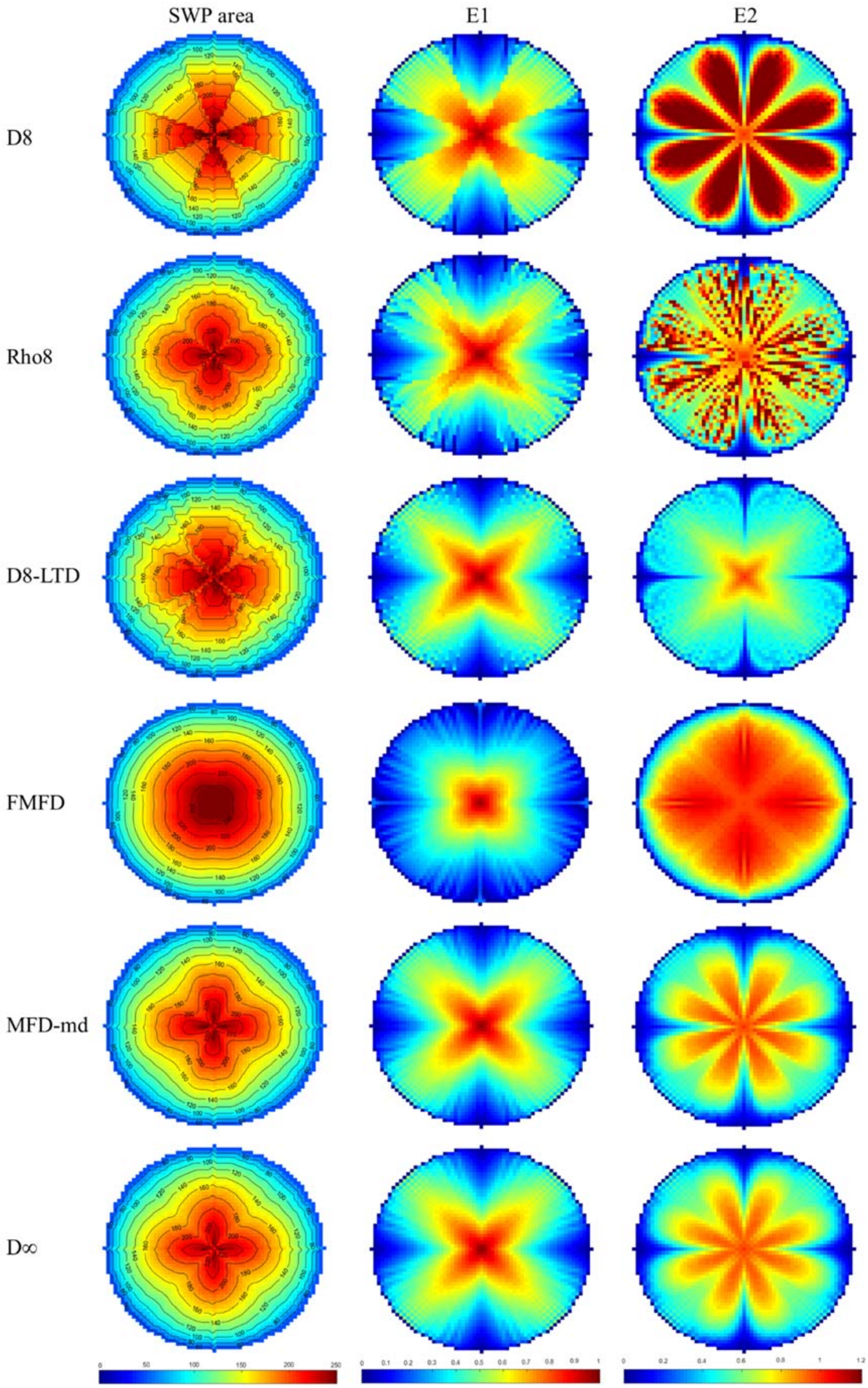
SWP area
E1
E2
D8
Rho8
D8-LTD
FMFD
MFD-md
D∞
0
50
100
150
200
250
0
0.1
0.2
0.3
0.4
0.5
0.6
0.7
0.8
0.9
1
0
0.2
0.4
0.6
0.8
1
1.2

Figure 7

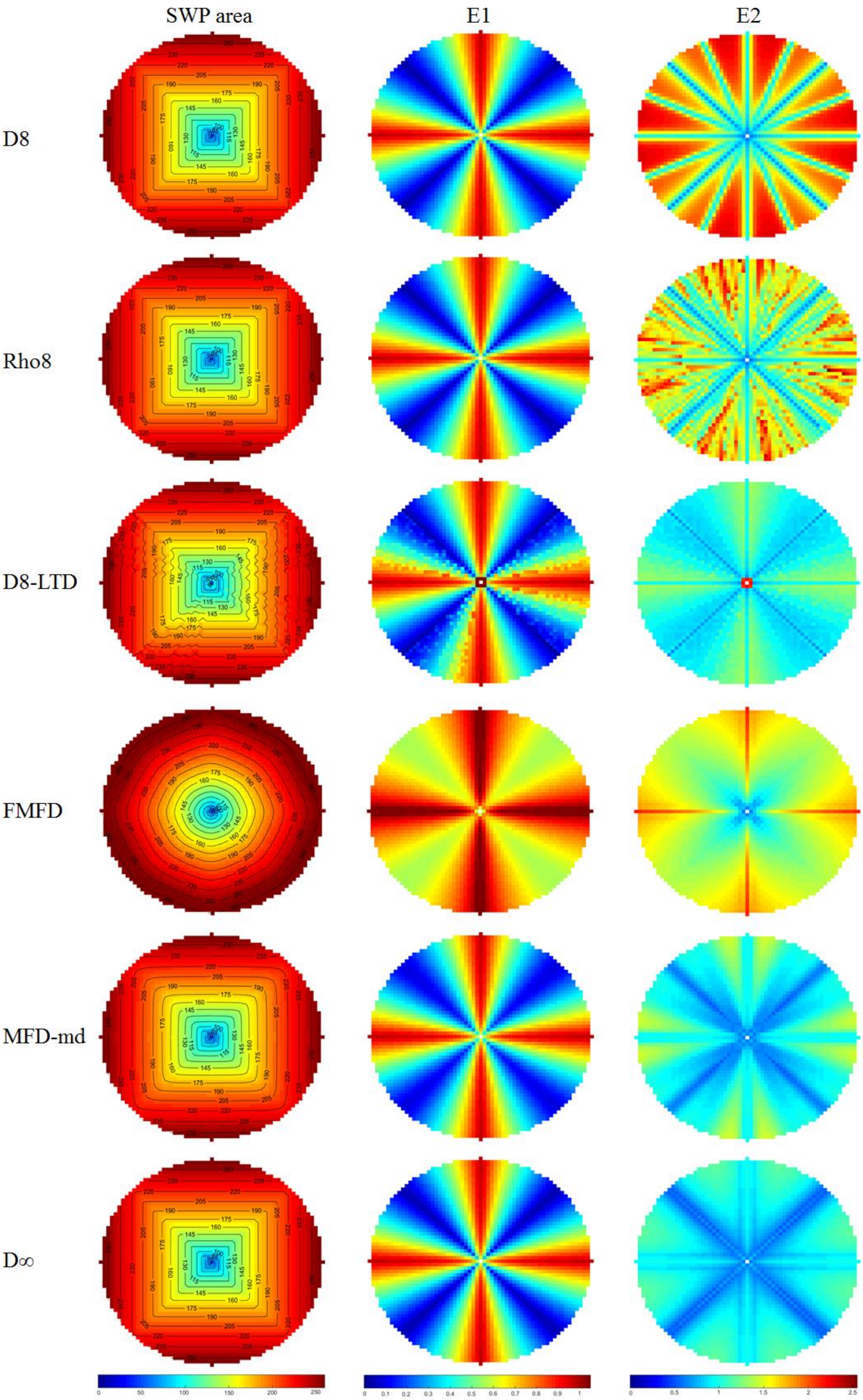

Figure 8

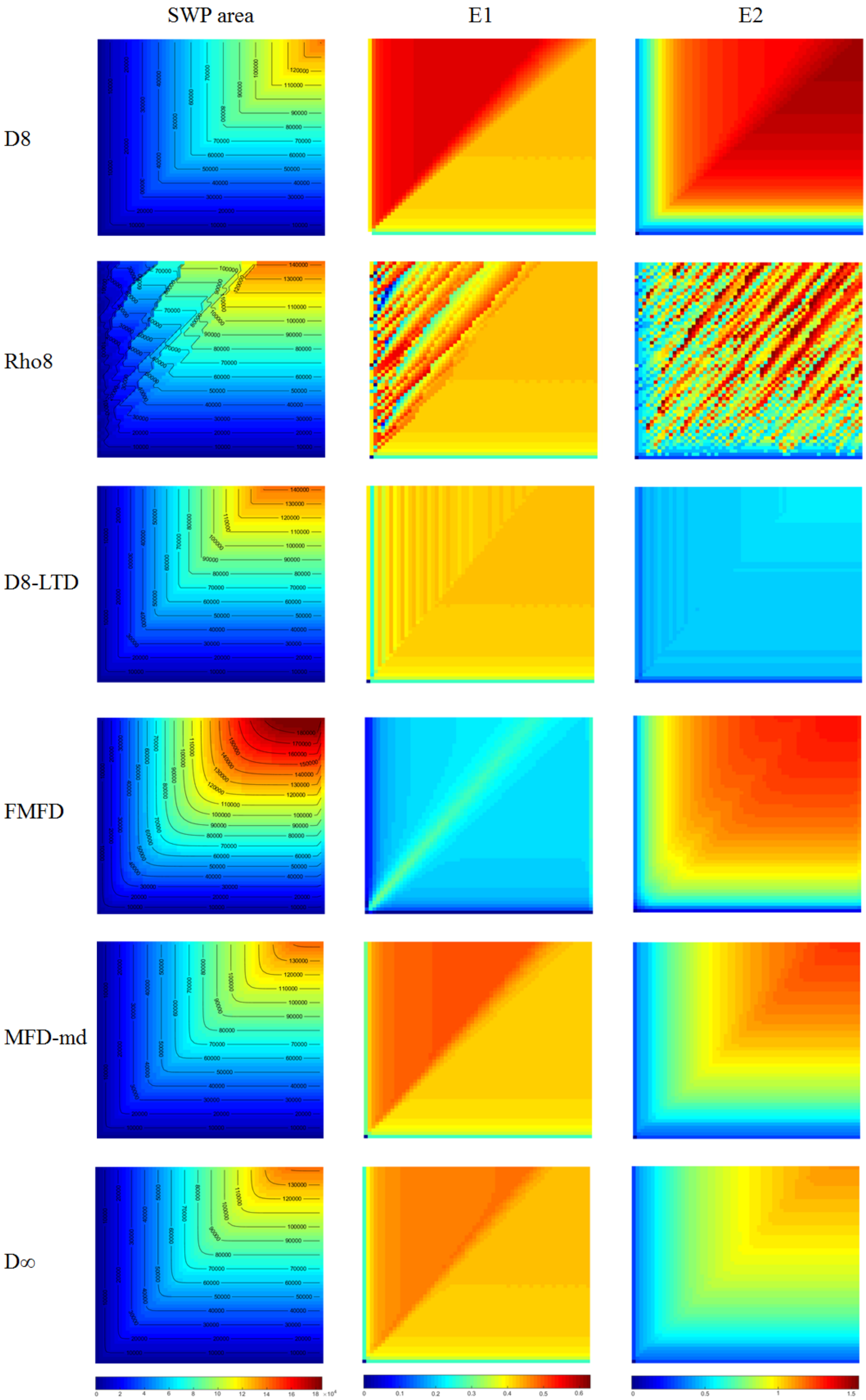

Figure 9

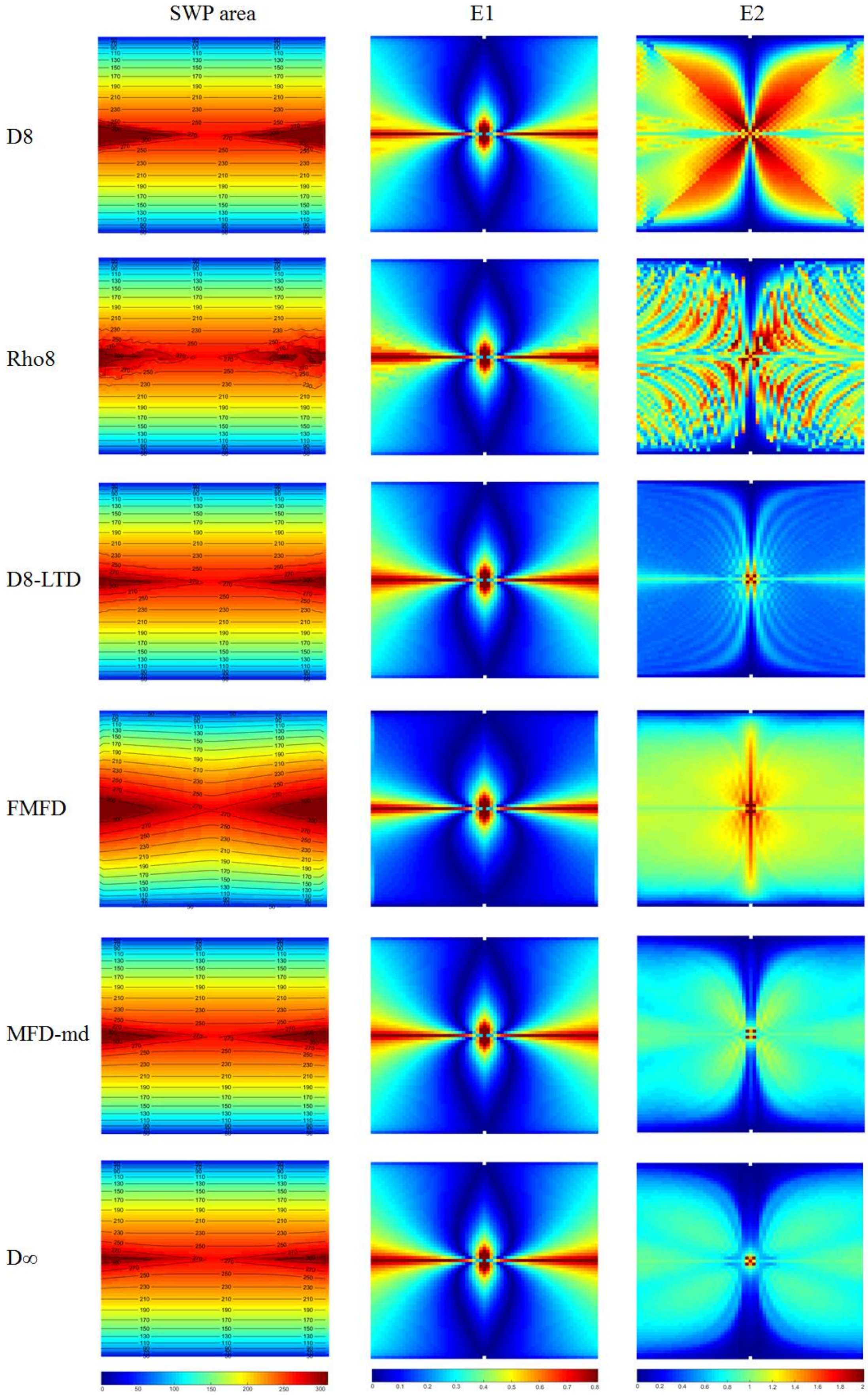

Figure 10

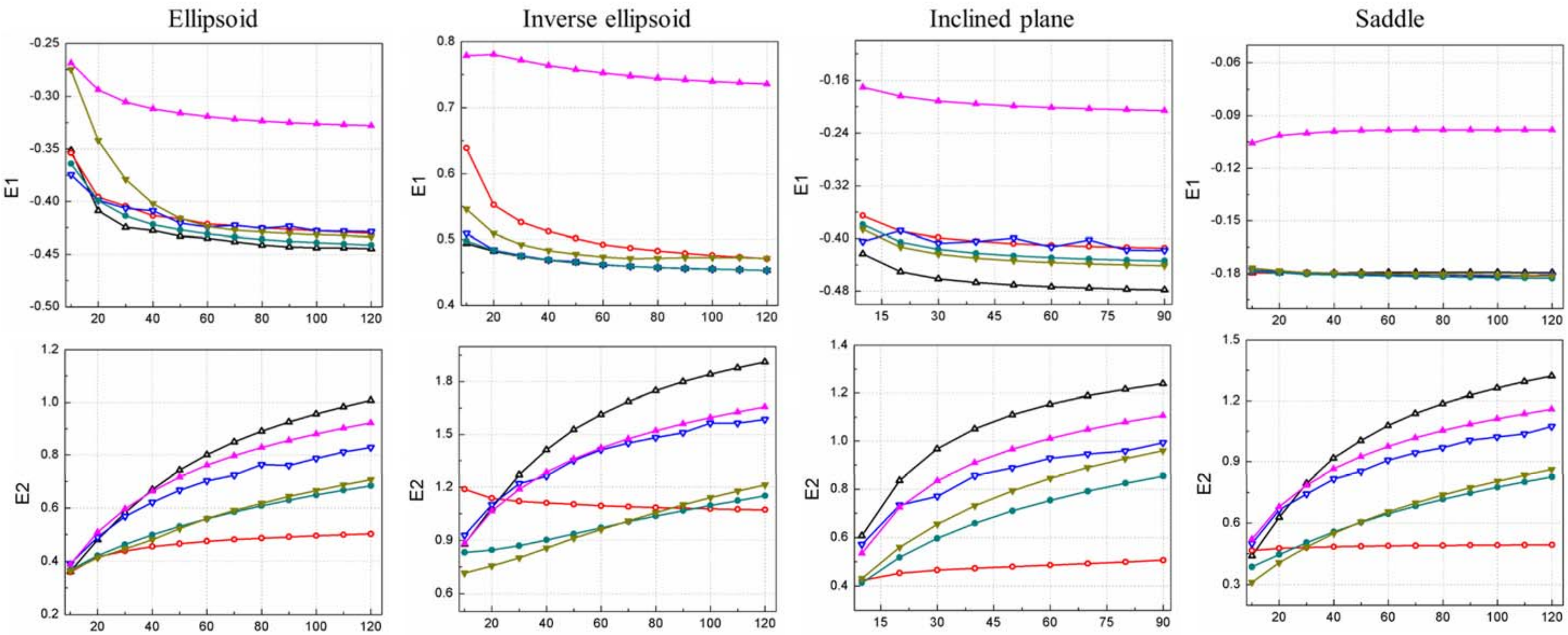
Ellipsoid
Inverse ellipsoid
Inclined plane
Saddle
E1
E2
-0.25
-0.30
-0.35
-0.40
-0.45
-0.50
0.8
0.7
0.6
0.5
0.4
-0.16
-0.24
-0.32
-0.40
-0.48
-0.06
-0.09
-0.12
-0.15
-0.18
1.2
1.0
0.8
0.6
0.4
0.2
1.8
1.5
1.2
0.9
0.6
1.4
1.2
1.0
0.8
0.6
0.4
1.5
1.2
0.9
0.6
0.3
20 40 60 80 100 120
15 30 45 60 75 90

Figure 11

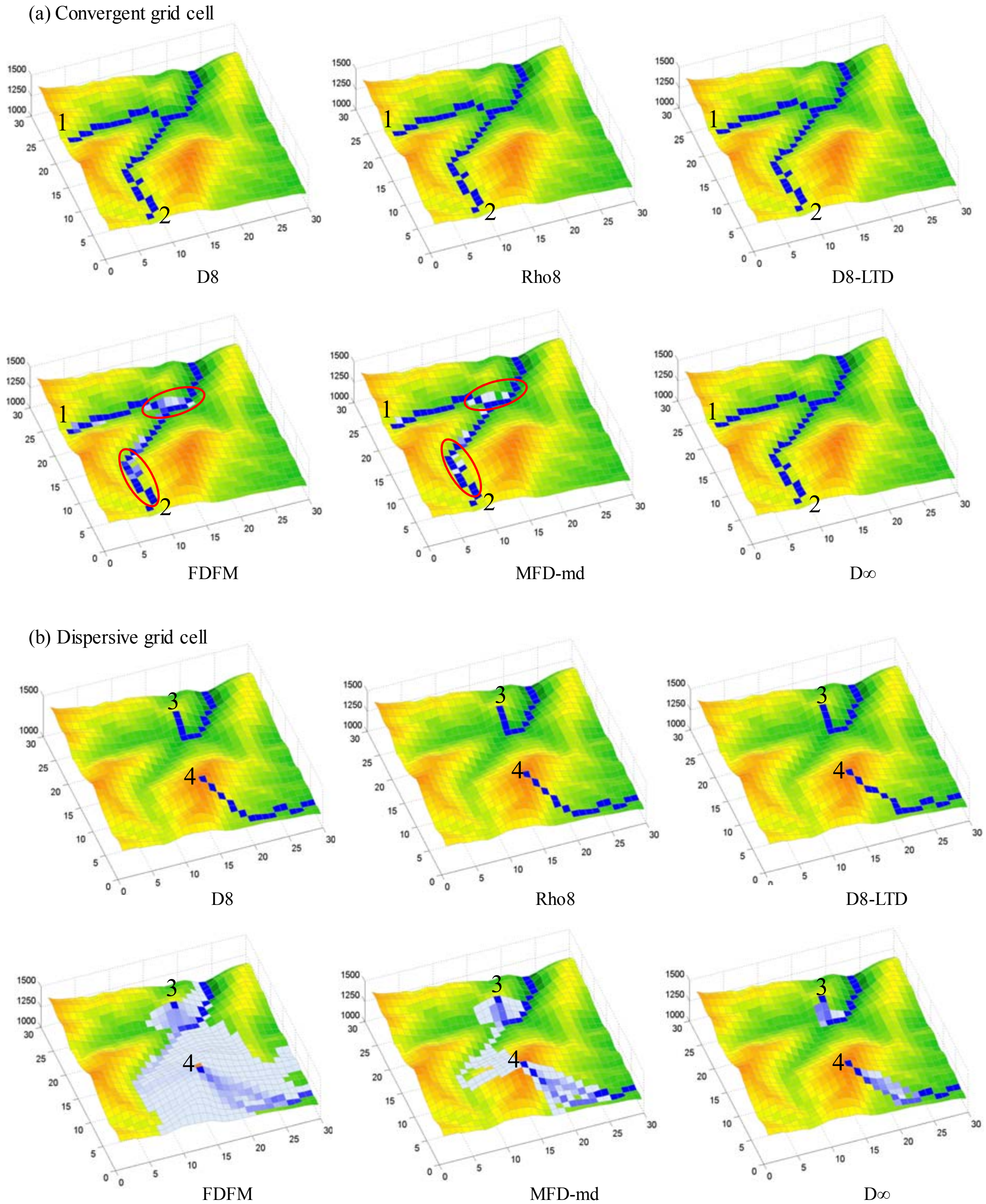

(a) Convergent grid cell
D8
Rho8
D8-LTD
FDFM
MFD-md
D∞
(b) Dispersive grid cell
D8
Rho8
D8-LTD
FDFM
MFD-md
D∞

*Declaration of Interest Statement

Declaration of interests

☒ The authors declare that they have no known competing financial interests or personal relationships that could have appeared to influence the work reported in this paper.

☐The authors declare the following financial interests/personal relationships which may be considered as potential competing interests:

Author contribution section:

Conceptualization, Zhenya Li and Tao Yang; Data curation, Zhenya Li; Formal analysis, Zhenya Li and Tao Yang; Funding acquisition, Tao Yang; Investigation, Tao Yang; Methodology, Zhenya Li and Bin Yong; Project administration, Tao Yang; Resources, Tao Yang; Software, Zhenya Li; Supervision, Tao Yang and Chong-Yu Xu; Validation, Tao Yang and Chong-Yu Xu; Visualization, Zhenya Li; Writing—original draft preparation, Zhenya Li; Writing—review and editing, Zhenya Li and Chao Wang